Nanoscale Advances

ROYAL SOCIETY OF CHEMISTRY

PAPER

View Article Online
View Journal | View Issue

Cite this: *Nanoscale Adv.*, 2025, **7**, 6145

Biogenic synthesis of ZnO NPs, CuO NPs, and ZnO/CuO nanocomposites for facile degradation of organic pollutants and biomedical applications

Hafiza Kainat Abid,[a] Abu Bakar Siddique, *[a] Azhar Abbas,[ab] Muhammad Ashraf Shaheen, [c] Akbar Ali, [d] Mashal Fatima,[a] Ashwag Shami,[e] Maymounah A. Alrayyani,[f] Fakhria A. Al-Joufi[g] and Mohammed A. Assiri[h]

The continuous increase in population and industrial activity in several areas, including textiles, leather, plastics, cosmetics, and food processing, produces harmful organic pollutants such as azo dyes, which are harmful to aquatic life and cause water pollution. The remediation of these dyes using photo-responsive metallic nanoparticles (NPs) has become a viable technique for the purification of water. This study synthesized ZnO NPs, CuO NPs, and ZnO/CuO nanocomposites using *A. nilotica* leaf extract. The NPs and NCs were characterized by UV-Vis spectroscopy, FTIR, SEM, EDX, ZP, and PXRD. All the nanomaterials showed energy bandgap in the UV and visible light region (2.15–3.00 eV) evidenced by Tauc's plots, successful capping of NPs by organic moieties, identified by FTIR, and crystallite size in the range of 13.72–16.82 nm, calculated by the PXRD data utilizing the Debye–Scherrer equation and quasi spherical shape analyzed by SEM. Compared to ZnO NPs and CuO NPs, ZnO/CuO NCs showed significantly increased photocatalytic performance of 96% for MB dye degradation and 93% for MO dye degradation in 100 min with rate constant (k) values of about 3.35×10^{-2} min^{-1} and 2.65×10^{-2} min^{-1}, respectively. The effect of catalyst dose, pH, water composition, and radical scavengers was also evaluated to optimize the conditions and propose a degradation mechanism and p–n heterojunction with Fermi level shifting for improved exciton generation. The biomedical importance of the ZnO/CuO NCs was assessed by the disc diffusion assay to check the antibacterial potential, and DPPH assay, TFC assay and TPC assay for antioxidant potential. All these studies, along with the reusability of the catalyst, demonstrated the appreciable catalytic efficacy of ZnO/CuO NCs for the water purification of industrial effluents.

Received 13th June 2025
Accepted 3rd August 2025

DOI: 10.1039/d5na00583c

rsc.li/nanoscale-advances

1. Introduction

Climate change is mostly caused by environmental pollution, with industries being the most significant contributors. The textile industry's dyeing process is a leading cause of water pollution. Pollutants such as heavy metal ions, organic dyes, and microorganisms have badly affected the environment and ecosystem due to improper disposal of wastewater.[1–3] Synthetic dyes such as azo dyes account for approximately 65–75% of all textile dye products. They pose a severe threat to public health due to their easy dispersion into the surrounding waterbodies and are hence considered micropollutants in aquatic environments.[4] Textile dyes in water can inhibit oxygenation and sunlight penetration, disrupting aquatic life and photosynthesis in plants and algae.[5]

Removal of dyes and contaminants from wastewater has become more challenging in recent years.[6] Many physical and chemical processes have been used to degrade azo dyes, such as adsorption, reverse osmosis, reductive degradation, and photocatalysis.[7,8] But these approaches are costly, ineffective, and require high energy. On the other hand, biogenic synthesis is a non-toxic and viable method for producing NCs with enhanced photocatalytic and biological properties.[9,10] However, synthesizing nanomaterials utilizing microorganisms is

[a]*Institute of Chemistry, University of Sargodha, Sargodha 40100, Pakistan. E-mail: abubakar.siddique@uos.edu.pk*

[b]*Department of Chemistry, Government Ambala Muslim College, Sargodha 40100, Pakistan*

[c]*Department of Allied Health Sciences, The Superior University Lahore, Sargodha-Campus, 40100, Pakistan*

[d]*Department of Chemistry, Government College University Faisalabad, 38000-Faisalabad, Pakistan*

[e]*Department of Biology, College of Science, Princess Nourah bint Abdulrahman University, P. O. Box 84428, Riyadh 11671, Saudi Arabia*

[f]*Chemistry Department, Faculty of Science, King Abdulaziz University, PO Box 80203, Jeddah 21589, Saudi Arabia*

[g]*Department of Pharmacology, College of Pharmacy, Jouf University, 72341 Aljouf, Saudi Arabia*

[h]*Department of Chemistry, Faculty of Science, Research Center for Advanced Materials Science (RCAMS), King Khalid University, P. O. Box 960, Abha, 61421, Saudi Arabia*

difficult due to the complexity of isolating and maintaining cell cultures, as well as the various purification stages required. Thus, plant materials are used to synthesize NPs due to their easy availability. Also, biogenic synthesis is cost-effective and less hazardous than biosynthesis using fungal and bacterial sources.[11]

Nanotechnology has gained popularity over the past 20 years due to the remarkable capabilities of nanomaterials, which range in size from 1 to 100 nm. These nanomaterials have been extensively used to break down pollutants and protect the environment.[12] Zinc and copper oxides are examples of nontoxic metal oxides with various biological applications. These NPs have a large surface area, and when they are mixed, such as in a nanocomposite (NC), they result in materials with an increased surface area, larger reactive sites, higher electron and mass transfer, and improved efficiency.[13,14] Previously, ZnO NPs, CuO NPs, and ZnO/CuO NCs have demonstrated excellent photocatalytic properties against several organic pollutants.[15] CuO is a p-type semiconductor having a low bandgap of 1.4 eV, whereas ZnO is an n-type semiconductor with a bandgap of 3.3 eV.[16–18] Both these nanomaterials have several applications in photocatalysis. ZnO/CuO NCs show excellent properties because of their p–n characteristics, high humidity sensitivity, and broad light absorption.[16] However, the efficiency of these nanomaterials depends on the particles' size, shape, stability, capping agent, concentration, exposure period, biocompatibility, and pH.[19,20] Metal oxide NPs and their NCs obtained by green synthesis are found to be significantly more effective for antibacterial and photocatalytic applications than chemically synthesized nanomaterials.[21] Therefore, an investigation of heterojunctions based on ZnO/CuO NCs obtained by green synthesis will be an interesting aspect.

During photocatalytic reactions, the photocatalyst absorbs sunlight and degrades environmental toxins such as aquatic and atmospheric pollutants. Photodegradation has advantages over other conventional wastewater treatment technologies, as it can completely degrade organic contaminants in a few hours at room temperature. Furthermore, organic pollutants can be converted into non-hazardous products like water and carbon dioxide.[22] The photodegradation of organic pollutants is facilitated in the presence of nano-catalysts under sunlight due to the generation of reactive oxygen species (ROS) in the aqueous system when NPs are exposed to sunlight.[23] In the presence of suitable light, equivalent or higher in energy than the energy bandgap, the valence electrons of NPs are excited to the conduction band. It results in the generation of excitons (electron–hole pairs) in the system, which are actively involved in direct redox reactions with pollutants or produce secondary reactive species, like superoxide ion radicals, hydroxyl radicals, hydrogen peroxide, *etc.* These ROS can decompose the stable organic pollutants (*i.e.*, azo dyes) without the addition of any additional oxidants.[24] However, owing to the short life of excitons, the photodegradation is severely suppressed in the case of chemically synthesized and pristine NPs. Therefore, the generation of various heterojunctions to improve the life span of excitons and increase the generation of ROS is an interesting area, so that activity can be enhanced and organic pollutants can be degraded easily in a shorter time. Moreover, the stability and particle size improvements are also advantageous properties of the green synthesis of heterojunctions.[19] Hence, the current research work has been designed for the biogenic synthesis of pristine ZnO and CuO NPs, and their heterojunction (ZnO/CuO NCs) to assess the comparative photocatalytic activities and superiority over the previous reported literature.

Recently, the green synthesis of ZnO NPs, CuO NPs, and ZnO–CuO NCs has gained considerable attention due to their stability and broad-spectrum applications in photocatalysis and the biomedical field.[25–27] By the capping of phytochemicals, the surface moieties of NPs greatly influence the optical properties and size of NPs.[28,29] Therefore, various plants are being tried for the green synthesis of metal NPs. *A. nilotica*, a plant with medicinal properties, contains various phytochemicals such as triterpenoids, flavonoids, polyphenols, terpenoids, vital oils, tannins, saponins, steroids, and fatty acids. Its primary insecticidal component, azadirachtin, has antibacterial, antiviral, and anticancer properties. Flavonoids and polyphenols like kaempferol and quercetin have anti-inflammatory, anti-cancer, and antioxidant properties. Terpenoids, such as gedunin and azadiradione, have anti-inflammatory and antifungal properties.[30,31] Because of the special phytochemistry, the NPs and NCs obtained by green synthesis are expected to be good biomedical agents. The NPs obtained by green synthesis have been currently used in multiple biological applications, like tissue engineering, antimicrobial coatings, targeted medication delivery, and diagnostics.[32]

In this study, ZnO NPs, CuO NPs, and ZnO/CuO NCs were synthesized using *A. nilotica* leaf extract, which acts as a capping and reducing agent. These nanomaterials were successfully characterized and tested for their catalytic ability to decompose toxic dyes such as MB and MO. The effect of parameters, catalyst dose, pH, water composition, radical scavengers, and catalyst reusability was studied to check the actual wastewater treatment and deduce the degradation mechanism. Based on experimental results, a suitable heterojunction formation has been proposed for improved exciton generation. Moreover, the biological properties of the NPs have also been assessed by disc diffusion assay, DPPH assay, TFC assay, and TPC assay.

2. Experimental procedure

2.1. Materials and instruments used

A brief description of the chemicals and instruments used has been provided in the SI under the heading S1.

2.2. Preparation of leaf extract

The previously reported procedure was followed for the preparation of the leaf extract of *A. nilotica*.[33,34] Fresh *A. nilotica* leaves were washed thrice with DW to remove dust and other impurities, before being dried at ambient temperatures for 5 days. Subsequently, these leaves were crushed into a fine powder with a grinder. After that, 5 g of *A. nilotica* leaf powder was mixed with 100 mL of distilled water in a round-bottom flask and

stirred for 4 h at 120 °C. After filtration to remove undissolved materials, the extract was utilized to synthesize the nanomaterials. A glass Petri dish (150 mm × 15 mm) was used to dry the filtered liquid in an oven set at 50 °C. The dried plant extract was stored in an airtight jar and refrigerated at 4 °C for further work.

2.3. Preparation of ZnO NPs and CuO NPs

To prepare pristine metal oxide NPs, 0.5 M solution of $Zn(NO_3)_2 \cdot 6H_2O$ (0.5 g in 10 mL DW) and $CuCl_2$ (0.6 g in 10 mL DW) was prepared in separate beakers. Then, 4 mL of plant extract was added to each salt solution at a constant temperature of 80 °C with continuous stirring at 400 rpm, respectively. To maintain the basic pH (pH = 9) of reaction mixtures, the pH of both solutions was raised by adding drops of 1 M NaOH solution after every 5 minute interval. Formation of white colored precipitates in the zinc salt solution and black colored precipitates in the copper salt solution indicated the preparation of NPs and hydroxides of salts. These NPs were separated using centrifugation, washed with DW, pulverized with a mortar and pestle, followed by calcination at 350 °C for 3 h, which resulted in the synthesis of ZnO NPs and CuO NPs. These NPs were stored in Eppendorf tubes covered with aluminum foil and placed in a cool place to avoid exposure to sunlight.

2.4. Preparation of the ZnO/CuO NC-based heterojunction

For biogenic synthesis of ZnO/CuO NCs, 0.5 M $Zn(NO_3)_2 \cdot 6H_2O$ and 0.5 M $CuCl_2$ solutions were prepared in separate beakers. *A. nilotica* extract (4 mL) was gradually added to the above solutions (each solution of 10 mL) and stirred at 80 °C for 10 min. Subsequently, both solutions were combined, and the pH was adjusted to 9 with constant stirring. The resulting powder was stirred for 1 h at 80 °C, cooled to room temperature, and rinsed three to four times with DW. The supernatant was removed, and the residues were oven dried (100 °C for 5 h), followed by crushing of the powder and calcination at 350 °C for 3 h, resulting in the formation of a heterojunction.

2.5. Photocatalytic activity of ZnO NPs, CuO NPs, and ZnO/CuO NCs

The photodegradation of azo dyes was carried out under sunlight using biosynthesized ZnO NPs, CuO NPs, and ZnO/CuO heterojunction, following the reported literature.[35] To do this, 5 mg of MB and 5 mg of MO dye were dissolved in 500 mL of distilled water to obtain a 10 ppm solution for each dye in two separate beakers. 20 mL of the solution of each dye was combined with 30 mg of biosynthesized ZnO NPs, CuO NPs, and ZnO/CuO NCs. The reaction suspension was thoroughly mixed in the absence of sunlight to bring the working solution to adsorption–desorption equilibria before sunlight exposure. Afterward, the solutions were exposed to sunlight (dated: 25 June 2024) at the University of Sargodha for 100 min. The UV-visible spectra of the samples were recorded every 10 min to assess the degradation of dyes (%) using eqn (1).[36]

$$\text{Degradation of azo dye}(\%) = \frac{A_o - A_f}{A_o} \times 100 \quad (1)$$

A_o and A_f denote the initial and final absorbance of the solution, respectively.

The degradation data were fitted to a pseudo-1st order kinetic equation (eqn (2)) to determine rate constant values of the degradation reactions and compare the efficacies of the catalysts. The slope of the $\ln(C_o/C_t)$ *vs.* time (t) plot was used to calculate the rate constant (k).

$$\ln\frac{C_o}{C_t} = kt \quad (2)$$

The effects of pH (3–11), catalyst dose (10–50 mg), spiked water samples of different compositions (spiked tap water (TW) from the Analytical Chemistry Lab of the University of Sargodha, spiked river water (RW) from the Jhelum River), and radical scavengers were studied for optimization of the reaction conditions, real-time applications and proposal of the degradation mechanism.

2.6. Biomedical applications

The antibacterial potential of the NPs and NCs was assessed by the standard disc diffusion assay, following the procedure that was reported earlier.[5,37] Briefly, 2 mg mL^{-1} of each sample was sonicated in water and applied to sterile paper discs. These discs were placed in bacteria-seeded nutrient agar Petri dishes and incubated for 24 h at 37 °C. The zone of inhibition of each disc was measured in millimeters.

For the antioxidant activity of ZnO/CuO NCs, the standard DPPH (1,1-diphenyl-2-picrylhydrazyl) assay, TFC (total flavonoid content) assay, and TPC (total phenolic content) assay were utilized, as reported in our previous work.[38]

For the DPPH assay, the DPPH radical scavenging ability of ZnO/CuO NCs and ascorbic acid as a standard was assessed by adding different concentrations of samples (100–500 μg mL^{-1}) in 3 mL of ethanolic DPPH solution (4 mg/100 mL). After incubation for 30 min in the dark, the decrease in absorbance of solutions at λ_{max} of 517 nm was recorded and used to calculate the DPPH radical scavenging activity (%).

For the TPC assay, various concentrations of ZnO/CuO NCs (100–500 μL; 1 mg mL^{-1}) were added to 250 μL of 1 N Folin–Ciocalteu's phenol solution in 2 mL DW. Afterward, each sample was mixed with 750 μL of 20% Na_2CO_3 solution along with the addition of 950 mL of DW. After incubation for 30 min, the absorbance of each solution was measured at 765 nm. The results of TPC assay were reported in comparison to standard gallic acid as μg (GAE μg mL^{-1}).

For the TFC assay, the various concentrations of ZnO/CuO NCs (100–500 μL; 1 mg mL^{-1}) were mixed with 0.75 mL methanol, and the volume was raised to 2 mL by the addition of DW, followed by the addition of 300 μL of 10% $AlCl_3$ solution and 5% $NaNO_3$ solution. By increasing the volume of the mixture to 5 mL by adding 1 M NaOH solution and incubating for 40 min,

the absorbance of the samples was recorded at 510 nm. The results of TPC assay are reported in comparison to standard gallic acid as μg (QCE μg mL^{-1}).

2.7. Statistical treatment of data

All the photocatalytic, antimicrobial, and antioxidant experiments were performed thrice, and results have been reported as mean ± SD. All the results were analyzed statistically using ANOVA. Statistical significance was accepted at a level of $p < 0.05$.

3. Results and discussion

The aqueous leaf extracts of various plants are enriched with phytochemicals, like polyphenols, terpenoids, alkaloids, *etc.* These bioactive compounds have the ability to reduce and stabilize the NPs, as reported by various studies.[9] The phytochemical analysis of the aqueous leaf extract of *Acacia nilotica* was performed using various tests, as reported in the literature. The qualitative phytochemical screening tests of the aqueous leaf extract of *Acacia nilotica* showed the presence of phenolics, flavonoids, alkaloids, and carbohydrates in the sample, as illustrated in Table S1. Based on this, it was anticipated that this extract might be used as a reducing and capping agent of NPs and NCs.

3.1. UV-visible, FTIR, and zeta potential (ZP) analysis

Fig. 1a–c shows the UV-Vis spectra of pristine NPs and NCs after sonication of the samples for 10 min in DW. The absorbance spectrum of the aqueous extract of *A. nilotica* was also recorded and is shown in Fig. S1. *A. nilotica* exhibits multiple UV-visible absorption peaks of almost equal absorbances in the range of 300–430 nm, while the distinct maximum absorption bands for ZnO NPs, CuO NPs, and ZnO/CuO NCs were seen at 351 nm, 327 nm, and 322 nm, respectively, as illustrated in Fig. 1a–c. The lower absorption maximum value of NCs as compared to pristine NPs could be linked to the coupling of several metal oxide energy levels to produce a new energy level, or due to the formation of defect energy levels inside NCs.[39]

The optical band gaps (E_g) of the NPs and NCs were determined using Tauc's plot for the direct transition by extrapolating the straight line of the $(\alpha h\nu)^2$ *vs.* "$h\nu$" graph, plotted by using eqn (3).[40]

$$(\alpha h\nu)^n = A(h\nu - E_g) \quad (3)$$

Planck's constant, frequency, an energy-independent constant, the absorption coefficient, and the kind of transition are represented by h, ν, A, α, and n, respectively. The E_g values for ZnO NPs, CuO NPs, and ZnO/CuO NCs were calculated to be about 3.00 eV, 2.15 eV, and 2.56 eV, respectively, using Tauc's plot shown in the inset of each spectrum presented in Fig. 1a–c. ZnO NPs have a higher band gap as compared to ZnO/CuO NCs, indicating that increasing the amount of CuO in NCs lowers the energy band gap. For improved photocatalytic activity of NPs and NCs, the E_g must fall in the visible region, in addition to the large surface area.[41] Both these properties play a decisive role in the catalytic efficacy of materials.

FTIR spectra of the samples were recorded to analyze the functional groups involved in the stabilization of pristine NPs and ZnO/CuO NCs. Fig. 1d shows the FTIR spectra of the plant

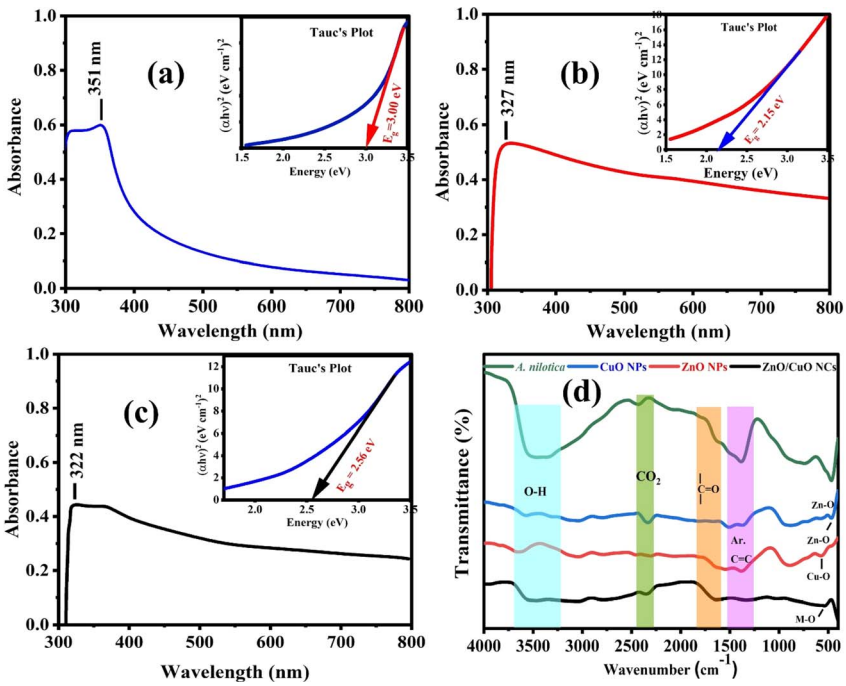

Fig. 1 UV-Vis spectra of (a) ZnO NPs, (b) CuO NPs, (c) ZnO/CuO NPs, (d) comparative FTIR of the extract, ZnO NPs, CuO NPs, and ZnO/CuO NCs.

extract and biosynthesized nanomaterials, which were recorded in the range of 4000 to 400 cm^{-1}. The FTIR analysis revealed potential functional groups (hydroxyl, carbonyl, phenolics, *etc.*) involved in the reduction, capping, and production of nanomaterials. The broad band ranging from 3643 to 3200 cm^{-1} observed in all spectra is attributed to the O–H stretching frequency due to the presence of polyphenols on the surface and water molecules on the surface of the synthesized NPs and NCs. The peaks at 1640–1730 cm^{-1} and 1480 cm^{-1} indicated the presence of the carbonyl group and aromatic C=C stretching.[42] The peaks at 480 cm^{-1} and 523 cm^{-1} represented the Zn–O and Cu–O stretching vibrations. The FTIR spectrum of ZnO/CuO NCs displayed a peak at 538 cm^{-1}, assigned to M–O bonds, which are attributed to Zn–O and Cu–O bonds in the heterojunction.

The surface charge of the NPs and NCs significantly influences the aqueous stability and adsorption potential of the catalysts.[43] Larger the value of ZP, more stable the particles in aqueous media. The more negative charge on the surface, the greater is the adsorption of cations on the surface and *vice versa*. Hence, the catalytic phenomenon can be comprehensively evaluated by analyzing the ZP value. The ZP values of the biogenically synthesized NPs and NCs are depicted in Fig. 2. All the samples showed good stability with ZP > −30 mV. The ZnO NPs showed a ZP of −35.4 mV with an SD of 3.2 mV, relatively better than that of CuO NPs (ZP = −31.9 ± 3.8 mV), and ZnO/CuO NCs showed the best stability with a ZP value of −38.1 ± 2.2 mV. This fluctuation can be linked to the particle size variations of the NPs and NCs. Additionally, it can also be anticipated that the NCs will be highly stable with high adsorption capability for cationic dyes for photocatalytic applications.

3.2. PXRD analysis

PXRD spectra were used to assess the synthesis and crystallite parameters of biosynthesized nanomaterials in the 2θ range (30–70°). The resulting diffractograms are shown in Fig. 3. The ZnO NPs exhibited diffraction peaks at 2θ = 31.94°, 34.62°, 36.42°, 47.70°, 56.71°, 62.88°, and 68.067°, which correspond to miller indices (100), (002), (101), (102), (110), (103), and (112), respectively. These findings align with the monoclinic phase of the standard JCPDS card no. 036-1451 for ZnO NPs.[44] Similarly, Bragg's reflections at 2θ values of 32.97°, 35.63°, 38.77°, 48.87°, 53.51°, 58.37°, 61.68°, 66.40° and 68.18° correspond to miller indices (110), (−111), (111), (−202), (020), (202), (−113), (−311) and (220), respectively.[45] These planes are well in agreement with JCPDS no. 89-2531, which confirms the formation of CuO NPs. The PXRD spectrum of ZnO/CuO NCs showed the diffraction peaks of ZnO NPs at 2θ values with lattice planes at 31.64° (100), 34.41° (002), 36.21° (101), 47.56° (102), 56.51° (110), and 62.81° (103), along with the peaks of CuO NPs at of 32.62° (110), 35.44° (−111), 38.70° (111), and 67.86° (220). All these peaks confirmed the formation of the ZnO/CuO NC heterojunction.

The crystallite parameters were calculated from crystallographic relationships, like the Debye–Scherrer, dislocation density, microstrain, and degree of crystallinity equations (eqn

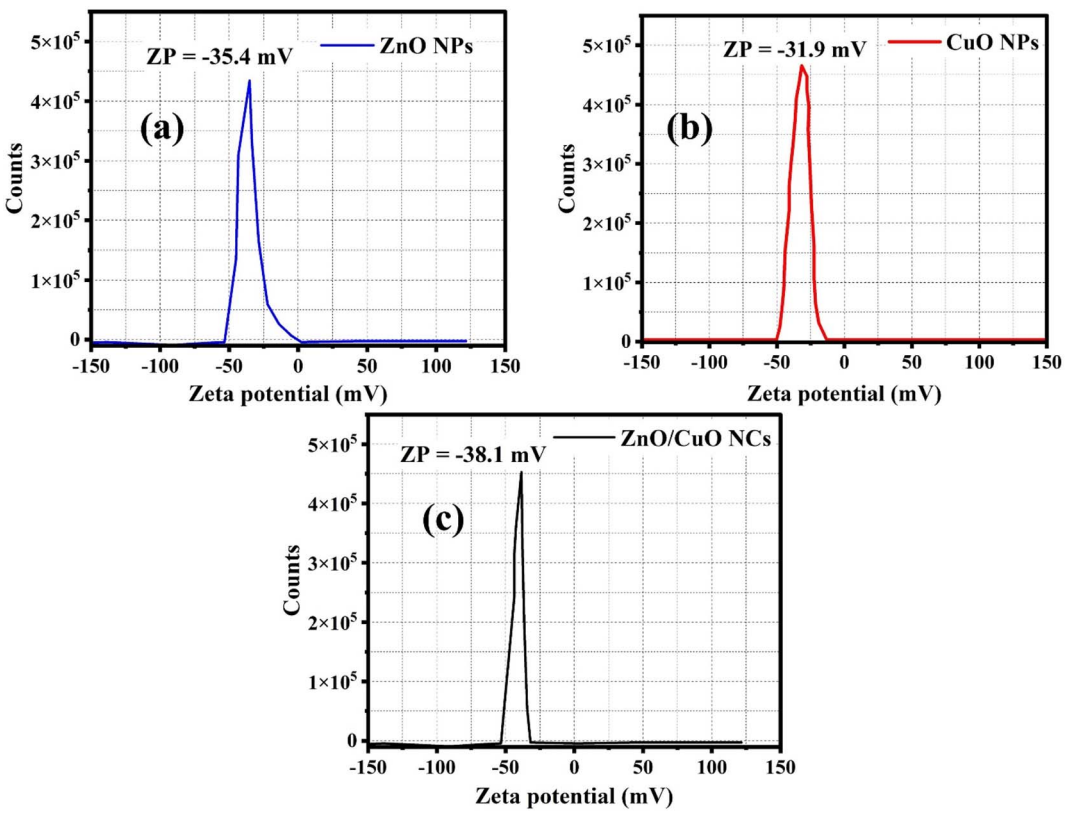

Fig. 2 ZP analysis of (a) ZnO NPs, (b) CuO NPs, and (c) ZnO/CuO NCs.

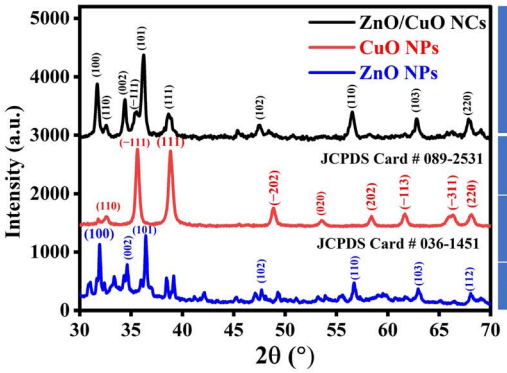

Sample	Average crystallite size 'D' (nm)	Dislocation density δ × 10⁻³ (nm⁻²)	Micro strain ε × 10⁻³	Degree of crystallinity (%)
ZnO NPs	14.94	4.47	0.60	44.35
CuO NPs	16.82	3.53	0.611	69.97
ZnO/CuO NCs	13.72	5.31	0.501	29.64

Fig. 3 PXRD spectra of nanomaterials along with the crystallite parameters of all samples.

(4)–(7)). The calculated parameters depicted in Fig. 3 show the smaller crystallite size of ZnO/CuO NCs (13.72 nm), in comparison to ZnO NPs (14.94 nm) and CuO NPs (16.82 nm), along with the smaller crystallinity of 29.64% in comparison to ZnO NPs (44.35%) and CuO NPs (69.97%). These parameters indicated the amorphous nature of all samples and the maximum surface area of ZnO/CuO NCs due to the minimum crystallinity and the smallest crystallite size among all samples.

$$D = \frac{k\lambda}{\beta \cos \theta} \quad (4)$$

$$\delta = \frac{1}{D^2} \quad (5)$$

$$\varepsilon = \frac{\beta}{4 \tan \theta} \quad (6)$$

$$\text{Degree of crystallinity} = \frac{\text{area of crystalline peaks}}{\text{area of all peaks}} \times 100 \quad (7)$$

Here, D, k, λ, β, and θ represent the crystallite size, Scherer constant or shape factor, X-ray beam wavelength, peak FWHM, and diffraction angle, respectively.

In addition to crystallite size and crystallinity (%), dislocation density and microstrain values of the samples were also calculated, which are important parameters to assess the mechanical and electrical properties. Generally, the dislocation density is inversely proportional to the crystallite size. The smaller the dislocation density, the higher the material strength and the greater the resistance to deformation under stress.[46] The highest value of dislocation density was displayed by ZnO/CuO NCs (5.31×10^{-3} nm^{-2}), which showed increased stiffness and potential plastic deformation may occur, as compared to pristine NPs. Moreover, the microstrain values indicate the level of strain within the material, which may affect the mechanical and optical properties, and electrical conductivity. A smaller value of microstrain was exhibited by ZnO/CuO NCs (0.501×10^{-3}), as compared to pristine NPs.

3.3. SEM and EDX analysis

Morphological and compositional analysis of the nanomaterials was carried out by SEM and EDX, as shown in Fig. 4. The SEM image of ZnO NPs showed that they have spherical shape morphology with little aggregation (Fig. 4a). They have particle size ranging from 50 to 130 nm, with an average value of 83.36 ± 13.44 nm, as indicated by the particle size histogram depicted in Fig. 4b. EDX analysis confirmed the high purity and the presence of Zn and O with weight percentages of 96.76% and 3.24%, respectively (Fig. 4c). The oxygen peak confirms that zinc is found in its oxidized form. The EDX results verify that the ZnO NPs were successfully synthesized and their composition is in accordance with the targeted stoichiometry.

Fig. 4d shows that CuO NPs exhibit good homogeneity, spherical form, and adequate separation. A homogeneous distribution of particles allows better determination of the particle size, as shown in Fig. 4e. The average diameter of CuO NPs was 99.63 ± 20.49 nm as calculated by plotting the histogram (Fig. 4e). The presence of Cu, O, C and Cl was confirmed by EDX analysis with copper being a prominent constituent along with organic functional groups on the surface (Fig. 4f).

Fig. 4g shows the shape and structure of the biosynthesized ZnO/CuO NCs using SEM with a predominantly spherical shape. The average particle size was found to be 64.57 ± 12.07 nm as depicted by the histogram (Fig. 4h). EDX analysis confirmed the presence of Cu, O, Zn, C, and Cl (Fig. 4i). Carbon traces were visible in these three spectra because the samples were biogenically synthesized using *A. nilotica* as the stabilizing agent.

For further confirmation of the particles' morphology in the case of ZnO/CuO NCs and their size distribution, the HR-TEM image was captured, as shown in Fig. S2a. The HR-TEM image showed the quasi-spherical shape of the particles with an average particle size of 61.90 ± 26.12, as depicted by the histogram (Fig. S2b).

In addition to the morphological analysis by HR-TEM, the surface area of the ZnO/CuO NCs (having the smallest particle size) was also estimated by Brunauer–Emmett–Teller (BET) surface area analysis by plotting the BET isotherm, as shown in Fig. S3. The N_2 adsorption–desorption isotherm of the biologically synthesized ZnO/CuO NCs exhibited a hysteretic loop consisting of a Type IV profile, indicating the mesoporous nature. Such porosity is essential in catalytic systems to promote surface accessibility and facilitate efficient pathways for diffusion of reactants and degradation intermediates. Based on the BET analysis, the specific surface area of the sample was

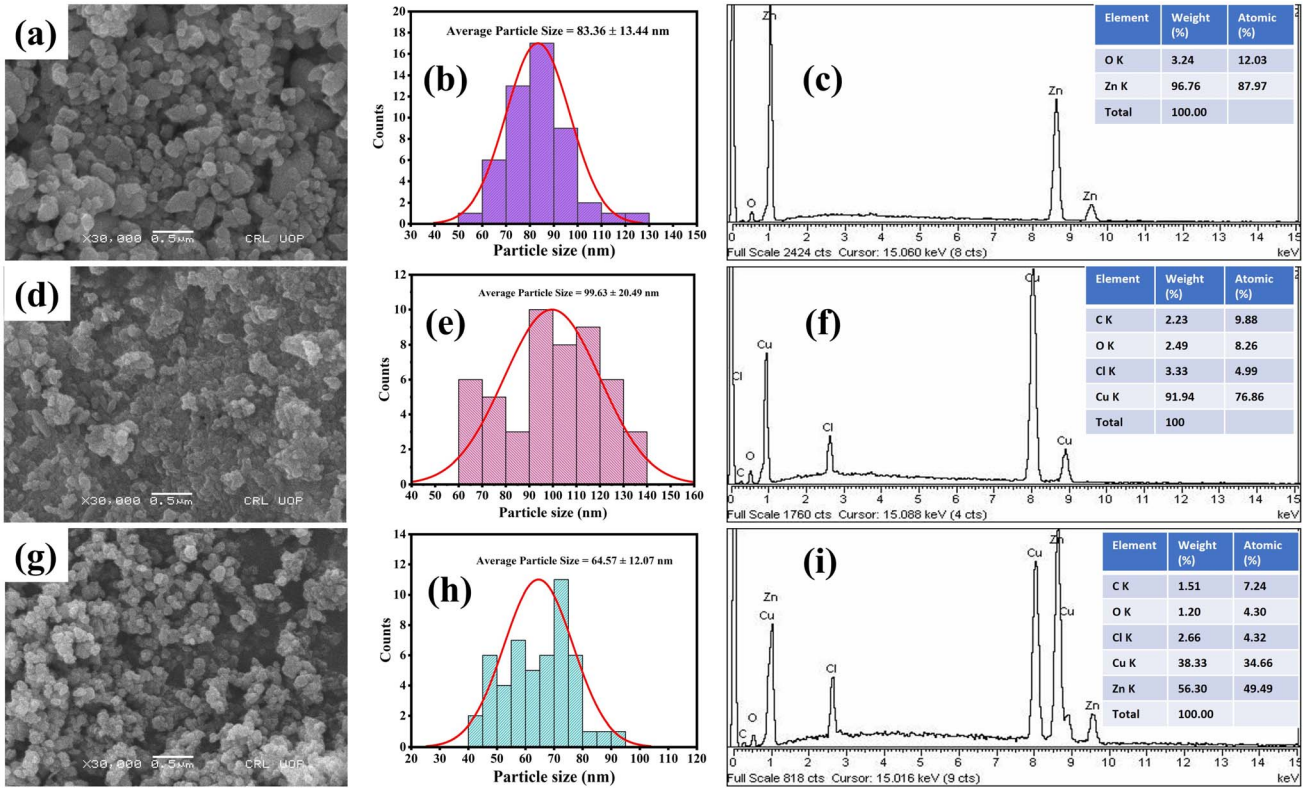

Fig. 4 (a) SEM image of ZnO NPs, (b) particle size histogram of ZnO NPs, (c) EDX energy spectrum of ZnO NPs, (d) SEM image of CuO NPs, (e) particle size histogram of CuO NPs, (f) EDX energy spectrum of CuO NPs, (g) SEM image of ZnO/CuO NCs, (h) particle size histogram of ZnO/CuO NCs, (i) EDX energy spectrum of ZnO/CuO NCs.

52.609 $m^2 g^{-1}$, suggesting a fairly high surface area that may be utilized in organic pollutant degradation and biomedical systems, with surface interaction being crucial. The fitting of the BET theory gave a slope of 82.3 ($1/g$), an intercept of −16.10 ($1/g$) and a constant (C) of −4.111, consistent with multilayer adsorption and surface heterogeneity, perhaps due to the mixed-phase structure, and biogenic synthesis. Such mesoporosity, combined with nanoscale size, may result in enhanced catalytic activity of ZnO/CuO NCs for the rapid degradation of organic dyes. Accordingly, the textural properties validate the multifunctional character of the prepared material that suits well for environmental as well as biomedical purposes.

3.4. Photocatalytic activities of pristine NPs and the heterojunction

The photocatalytic activity of biosynthesized nanomaterials was evaluated against MB and MO dyes for 100 min of visible light exposure. Fig. 5a and b shows the regular decrease in the absorbance of characteristic peaks of MB (Fig. 5a) and MO (Fig. 5b) after intervals of every 10 minutes. Using the absorbance values of characteristic peaks, the time-dependent photodegradation (%) of dyes using nanomaterials was measured using eqn (1). The results showed that MB and MO dyes rapidly degraded as exposure time increased for all samples until they became colorless or faded. The degradation efficiencies (%)

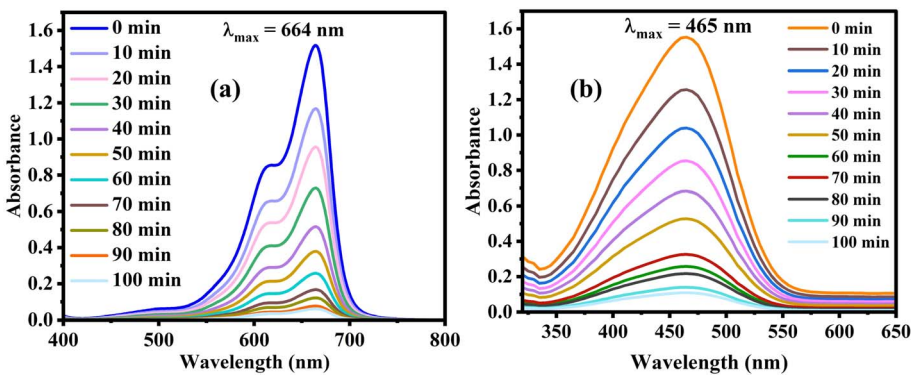

Fig. 5 Degradation spectrum of dye at different time intervals (a) MB and (b) MO.

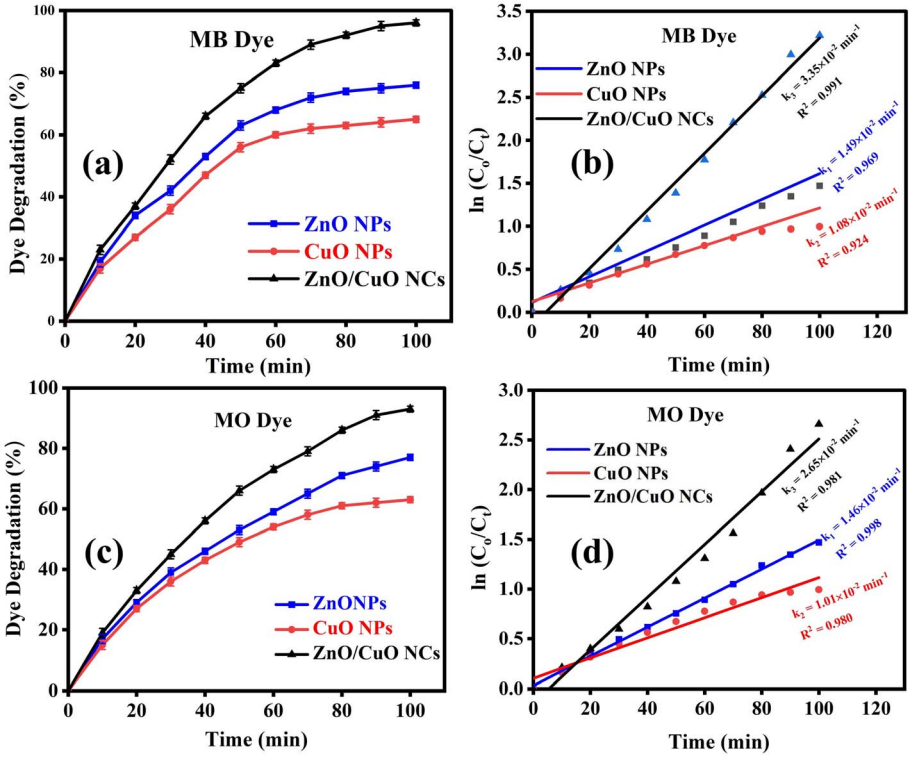

Fig. 6 Degradation efficiency *versus* time for (a) MB dye, (b) MO dye, (c) the reaction kinetics of MB dye (d) the reaction kinetics of MO dye. All results have been reported as mean ± SD, with number of replicates (n) = 3. Statistical significance was accepted at a level of $p < 0.05$.

measured were 96.0 ± 1.5%, 78.2 ± 1.0%, 63.1 ± 1.4% for MB dye (Fig. 6a) and 93.1 ± 1.25%, 78.3 ± 0.8%, 63.1 ± 1.3% for MO dye (Fig. 6b) by using ZnO/CuO NCs, ZnO, and CuO NPs, respectively. The change in MB and MO dye color and resulting degradation (%) was more noticeable in the presence of NCs than in pristine NPs. This can be anticipated due to the creation of a heterojunction by the mixing of oxides, which may significantly reduce the recombination of excitons and increase the visible region's photo-responsive range. To further understand the degradation process, kinetic investigations of the reaction were also conducted by fitting the degradation data into a pseudo-first-order kinetics equation, following eqn (2).

The kinetics data showed that the NC samples had significantly higher photocatalytic degradation rates than ZnO NPs and CuO NPs, as depicted in Fig. 6c and d. The rate constant values for ZnO/CuO NCs, ZnO NPs, and CuO NPs were calculated to be 3.35×10^{-2} min^{-1}, 1.49×10^{-2} min^{-1}, and 1.08×10^{-2} min^{-1}, respectively, for MB dye (Fig. 6c) and 2.65×10^{-2} min^{-1}, 1.46×10^{-2} min^{-1}, and 1.01×10^{-2} min^{-1}, respectively, for MO dye (Fig. 6d).

3.5. Effect of reaction variables on the catalytic efficiency of samples

The photocatalytic efficiency of a catalyst is greatly influenced by the reaction conditions, like catalyst dose, pH, matrix composition, and ROS inhibiting compounds. For the real sample analysis, reaction condition optimization, and proposed degradation mechanism, the catalyst efficiency was analyzed at various catalyst dosages, pH, water samples, and ROS inhibitors, by following the same method described earlier.[1]

The effect of ZnO/CuO NC dose (as depicted in Fig. 7a) showed that the catalytic efficiency increased with the increase in catalyst amount from 10 mg to 30 mg, due to the increase in surface area and active sites available for adsorbing dye molecules. With the further increase of ZnO/CuO NC dose (above 30 mg), the dye degradation (%) was reduced gradually, which might be due to an increase in the turbidity of the suspension, resulting in light scattering from surfaces and less penetration of light inside the reaction mixture to generate the excitons.

The effect of pH (depicted in Fig. 7b) showed anomalous behavior for MB and MO dye. With the increase of pH from 3 to 7, the catalytic activity of ZnO/CuO NCs was increased due to easy adsorption of cationic dye molecules on the surface and less inhibition of radicals by H^+ ions near neutral pH. With further increase of pH (at pH 9 and 11), the degradation efficiency was decreased because the hydrolysis of the catalyst may occur at high pH, resulting in the reduction of surface area and active sites. While in the case of MO, the same trend of degradation was observed at pH 9 and 11, below pH 7, the ZnO/CuO NCs showed better degradation of MO than MB. This trend was observed because MO is anionic in nature, and its adsorption efficiency increased with the decrease of surface negative charge, however, the overall reduction was observed due to the inhibition of ROS by high h^+ concentration.

The effect of various water compositions (Fig. 7c) showed the maximum dye degradation (%) in spiked DW due to the absence

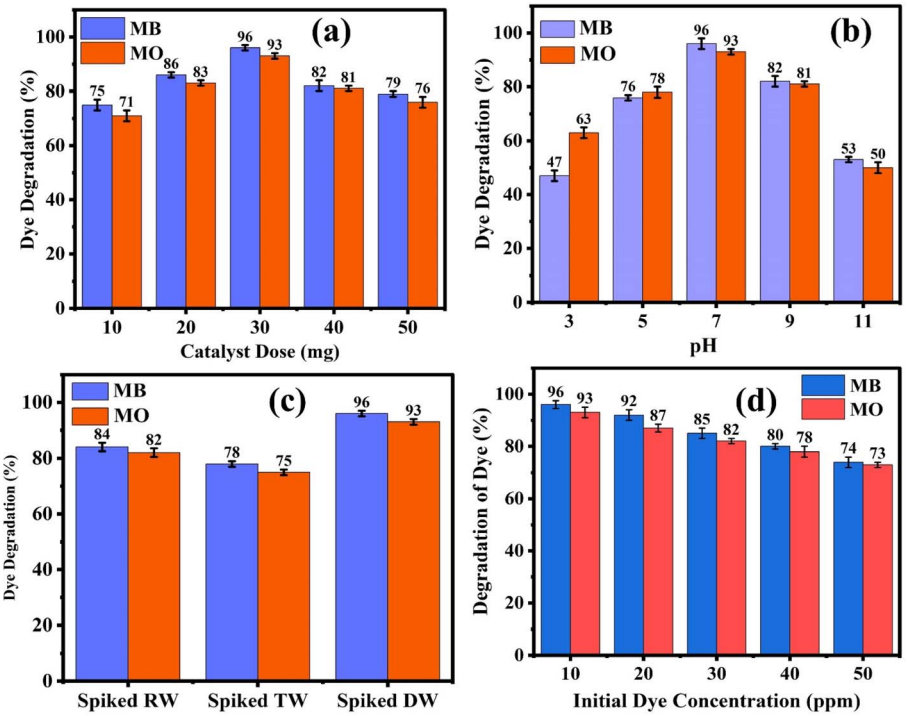

Fig. 7 Effect on dye degradation of various (a) catalyst doses, (b) pH values, (c) water matrixes, and (d) initial dye concentrations. All results have been reported as mean ± SD, with number of replicates (n) = 3. Statistical significance was accepted at a level of $p < 0.05$.

of any interferences. However, with the increase of hardness and impurities in spiked water samples, the degradation (%) was continuously reduced, as depicted by the higher degradation (%) of spiked RW than spiked TW.

The effect of initial concentration of dyes on the photodegradation ability of the ZnO/CuO NCs was studied to optimize the reaction conditions and degrade high concentrations of dyes. The results of the experiments (Fig. 7d) showed the gradual decrease in the catalytic efficiency of ZnO/CuO NCs with the increase of dye concentration. This decrease in degradation (%) in the given time (100 min) was observed due to the limited number of active sites on the catalysts' surface for the generation of ROS, resulting in the slower degradation of dye solutions. The decrease in degradation (%) may also be observed due to an increase in the turbidity of the mixture, resulting in less penetration of light for the photodegradation reaction on the catalyst surface.

The effect of radical scavengers (Fig. 8a) showed minimum involvement of superoxide ($O_2^{\bullet -}$) and hydrogen peroxide (H_2O_2) in the degradation process because minimum inhibition of dye degradation (%) was observed in the presence of L-ascorbic acid (L-AA), which acts as a H_2O_2 scavenger, and p-benzoquinone (p-BQ), which acts as an $O_2^{\bullet -}$ scavenger, while in the presence of isopropanol (IPA), which acts as an $^{\bullet}OH$ scavenger, the maximum inhibition of degradation (%) was observed followed by Na_2EDTA, which acts as a h^+ scavenger. These results

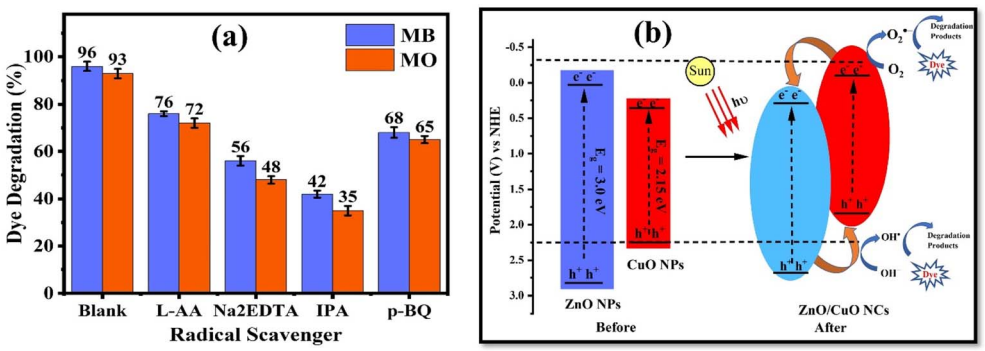

Fig. 8 (a) Effect of radical scavengers on dye degradation; (b) schematic illustration of band edge positions of E_{VB} and E_{CB} of ZnO NPs and CuO NPs, and proposed band alignment after the formation of a p–n heterojunction (ZnO/CuO NCs). All results have been reported as mean ± SD, with number of replicates (n) = 3. Statistical significance was accepted at a level of $p < 0.05$.

indicated the generation of all ROS in the reaction mixture and their active involvement in degradation. A degradation mechanism has been proposed based on these observations, as shown in S2 in the SI.

Based on the experimental evidence and theoretical calculations of band edge potentials (valence band (E_{VB}) and conduction band (E_{CB})) of ZnO NPs and CuO NPs,[22] it is suggested that there was a shifting of Fermi levels of ZnO NPs and CuO NPs, as shown in Fig. 8b. The Fermi level of ZnO NPs is lowered, and that of CuO NPs is shifted upward on the formation of a p–n heterojunction. As a result, the generation of $O_2^{\bullet-}$ and H_2O_2 is also facilitated in addition to the generation of $^{\bullet}OH$ and h^+. This shifting of Fermi levels also facilitated better absorption of sunlight. It lowered the recombination rate of electron–hole pairs, resulting in the better photocatalytic activity of the ZnO/CuO NC heterojunction for the degradation of azo dyes.[14] Moreover, the photocatalytic superiority of the synthesized ZnO/CuO NCs was also emphasized by comparison with the degradation rate constants of the previously reported materials, depicted in Table S2. The comparison table showed the improved photocatalytic potential of the ZnO/CuO NCs, as indicated by the high degradation constant values for azo dyes under sunlight. Hence, the current work has successfully reported ZnO/CuO NCs as improved photo-responsive photocatalysts for the remediation of azo dyes and water purification of industrial effluents.

3.6. Total organic carbon (TOC) analysis and reusability studies

The complete photodegradation of azo dyes to carbon dioxide and water, termed as mineralization under sunlight, is accomplished through a complex pathway. The color of the solution fades when the azo bond is broken down; however, the complete mineralization of the solution is a slow process and proceeds swiftly by completely degrading the organic species to water and carbon dioxide. The incomplete degradation may result in the generation of more reactive or toxic species, which may further deteriorate the water quality. Therefore, the TOC removal analysis of the azo dye solution was carried out to assess the extent of mineralization. The TOC removal (%) *vs.* time plot (Fig. 9a) depicted 83% and 82% mineralization of MB and MO dyes, respectively, after an exposure time of 4 h. These results demonstrated that the proposed catalyst (ZnO/CuO NCs) can effectively mineralize the azo dyes under sunlight and can be utilized to purify the water after long-term exposure, in contrast to only the disappearance of the color of the solution.

For reusability studies, the ZnO/CuO NCs with improved sunlight absorbance and photocatalytic performance were evaluated to degrade MB and MO spiked DW samples for five consecutive cycles batchwise. After each cycle, the ZnO/CuO NCs were recovered from the mixture by centrifugation, followed by drying in an oven at 80 °C for 3 h. The reusability studies showed a meager decrease in activity (~9%) after five cycles, as depicted in Fig. 9b. These observations proved the stability and reusable nature of the proposed catalyst with minimum effect on activity.

To verify he stability of the ZnO/CuO NCs after the 5th cycle of use, post-usage SEM, particle size histogram by SEM, and FTIR analysis of the sample were performed, as shown in Fig. S4. The SEM analysis revealed well-separated NPs with a quasi-spherical morphology, having an average particle size of 79.51 ± 10.75 nm, as shown in Fig. S4a and b, respectively. The slight increase in size was observed due to a small agglomeration of the particles after several uses, which might be responsible for the slight decrease in photocatalytic activity after five uses. To compare the surface functionalities of the NCs, the FTIR spectrum of the sample was compared before and after usage, as shown in Fig. S4c. The comparative spectrum showed that retention of almost all functional groups on the surface of NCs occurred even after five uses. These studies highlighted the potential of the synthesized material for repeated use.

3.7. Biomedical applications

The disc diffusion assay results (depicted in Fig. 10a) showed the more vulnerable nature of Gram-positive bacterial strains (*L. monocytogenes* and *S. epidermidis*) than Gram-negative bacteria (*P. aeruginosa* and *B. bronchiseptica*) by NPs and NCs. This activity trend can be attributed to the variation in the membrane barriers of both strains, since the Gram-positive bacteria have a thick peptidoglycan layer surrounding the

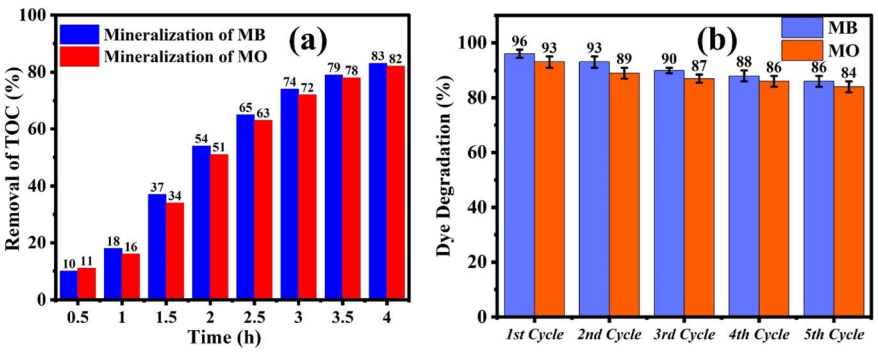

Fig. 9 (a) Removal of TOC (%) with time, (b) reusability studies of ZnO/CuO NCs to degrade azo dyes in spiked DW. All results have been reported as mean ± SD, with number of replicates (n) = 3. Statistical significance was accepted at a level of $p < 0.05$.

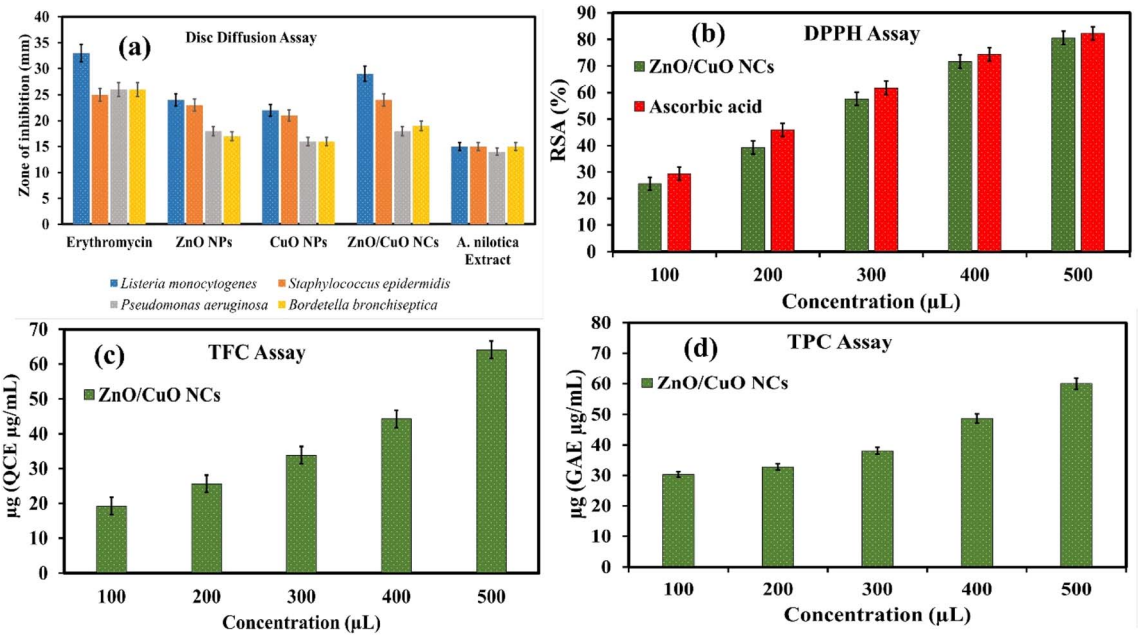

Fig. 10 Biological activity results of: (a) disc diffusion assay, (b) DPPH assay, (c) TFC assay, and (d) TPC assay. All results have been reported as mean ± SD, with number of replicates (n) = 3. Statistical significance was accepted at a level of $p < 0.05$.

cytoplasmic membrane. In contrast, the Gram-negative bacteria have lipopolysaccharide in the outer leaflet and a thin layer of peptidoglycan on the inner side; hence, it can be postulated that the NPs and NCs have less interaction with lipopolysaccharide than peptidoglycan, resulting in better activity against Gram-positive bacteria. Although the exact mechanism of action of NPs against microbes is still unknown, it has been reported earlier that the NPs inhibit bacterial growth by crossing the membrane barriers and interacting directly with the enzymes and genetic material, as well as by producing ROS in the vicinity and inside the bacteria.[1,41] The maximum inhibition of bacterial colonies by ZnO/CuO NCs (comparable to standard erythromycin) can be attributed to the smaller particle size and the easier generation of ROS compared to other nanomaterials.

The antioxidant activity of the ZnO/CuO NCs, assessed by the DPPH assay (Fig. 10b), TFC assay (Fig. 10c), and TPC assay (Fig. 10d) showed a gradual increase with the rise in concentration from 100 µL to 500 µL. The DPPH assay results showed that the radical scavenging ability (RSA (%)) became almost equal to that of standard ascorbic acid (80.3 ± 1.5%) at a concentration of 500 µL, as shown in Fig. 10b. The highest TFC value of 64.0 ± 1.1 µg (QCE µg mL^{-1}) was obtained in comparison to the highest TPC value of 60.0 ± 1.3 µg (GAE µg mL^{-1}), as shown in Fig. 10c and d, respectively. This appreciable antioxidant activity of ZnO/CuO NCs was attributed to the capping of biologically active metabolites (phenolics, flavonoids, terpenoids *etc.*) on the surface of NCs that synergistically enhance the antioxidant activity.[38]

4. Conclusion

Biogenically synthesised pristine ZnO NPs and CuO NPs, and the ZnO/CuO NC-based heterojunction using *A. nilotica* have been reported as cost-effective and eco-friendly photocatalysts for the remediation of organic pollutants. These nanomaterials were characterized by UV-Vis, FTIR, PXRD, ZP, SEM, and EDX analyses. UV-Vis spectra revealed improved sunlight absorption and better exciton separation in ZnO/CuO NCs than in pristine ZnO NPs and CuO NPs. FTIR showed the characteristic peaks of M–O bonds (490–540 cm^{-1}) and several functional groups (hydroxyl, carbonyl, aromatic rings, *etc.*) on the surface of nanomaterials as a capping agent. PXRD spectra revealed the characteristic diffraction lines of ZnO NPs, CuO NPs, and ZnO/CuO NCs with average crystallite sizes of 14.94 nm, 16.82 nm, and 13.72 nm, respectively. SEM analysis revealed the spherical shapes of NPs and NCs with particle diameters of 83.36 ± 13.44 nm, 99.63 ± 20.49 nm, and 64.57 ± 12.07 nm for ZnO NPs, CuO NPs, and ZnO/CuO NCs, respectively. When exposed to sunlight, these ZnO NPs, CuO NPs, and ZnO/CuO NCs showed good photocatalytic efficacy in degrading harmful azo dyes, like MB and MO. The degradation of MB dye was found to be 96.0 ± 1.5%, 78.2 ± 1.0%, and 63.1 ± 1.4% for ZnO/CuO NCs, ZnO NPs, and CuO NPs, with rate constant values of 3.35 × 10^{-2} min^{-1}, 1.4 × 10^{-2} min^{-1}, and 1.0 × 10^{-2} min^{-1}, respectively. Similarly, degradation (%) of MO dye was found to be 93.1 ± 1.25%, 78.3 ± 0.8%, and 63.1 ± 1.3%, with rate constant values of 2.65 × 10^{-2} min^{-1}, 1.4 × 10^{-2} min^{-1}, and 1.0 × 10^{-2} min^{-1} for ZnO/CuO NCs, ZnO NPs, and CuO NPs, respectively. The effect of reaction parameters showed the maximum degradation of dyes at a catalyst dose of 30 mg and pH 7 in spiked DW, along with the maximum inhibition of degradation in the presence of $^{\bullet}OH$ and h^{+} scavengers. A suitable degradation mechanism and generation of p–n heterojunction were proposed based on radical scavenging experiments. Reusability experiments confirmed the stable and reusable nature of ZnO/CuO NCs for wastewater treatment

applications. Conclusively, the proposed heterojunction-based photocatalyst can be optimized for commercial-scale applications with improved degradation capability under sunlight. Moreover, the biological evaluation of the ZnO/CuO NCs showed better inhibition of bacterial strains than pristine ZnO NPs and CuO NPs, as well as the extract. The antioxidant activity results showed the DPPH radical inhibition (%) of 80.3 ± 1.5, TFC of 64.0 ± 1.1 μg (QCE μg mL^{-1}), and TPC of 60.0 ± 1.3 μg (GAE μg mL^{-1}) by ZnO/CuO NCs. All these activities demonstrated the potential of these NCs for biomedical applications.

Author contributions

Hafiza Kainat Abid & Abu Bakar Siddique: methodology, investigation, writing – original draft, writing – review & editing. Azhar Abbas, Muhammad Ashraf Shaheen, & Akbar Ali: conceptualization, supervision, writing – review & editing. Mashal Fatima, Ashwag Shami, Maymounah A. Alrayyaniv, & Fakhria A. Al-Joufi: investigation, writing – review & editing. Mohammed A. Assiri: writing – review & editing.

Conflicts of interest

The authors have no known financial or non-financial interests to disclose.

Data availability

All evaluated data are available in the manuscript. Additional information/data can be provided upon reasonable request.

The supplementary information contains some additional data about the instruments used, phytochemical analysis of plant extract, UV-visible spectrum of extract, HR-TEM and BET analysis of ZnO/CuO NCs, comparison table and post-usage analysis of catalyst supporting the findings of this study. See DOI: **https://doi.org/10.1039/d5na00583c**.

Acknowledgements

The authors express their gratitude to Princess Nourah bint Abdulrahman University Researchers Supporting Project number (PNURSP2025R31), Princess Nourah bint Abdulrahman University, Riyadh, Saudi Arabia. The authors express their appreciation to the Deanship of Scientific Research at King Khalid University, Saudi Arabia, for this work through a research group program under grant number RGP-2/40/46.

References

1 H. Ahmad, A. B. Siddique, S. Zaheer, R. Sattar, A. Abbas, M. Amin, R. Al-Salahi, H. A. Abuelizz and M. Z. Saleem, *J. Water Process Eng.*, 2025, **74**, 107855.
2 A. Abbas, A. B. Siddique, R. Batool, M. Sher, M. I. Irfan and M. A. Abbas, *Starch/Staerke*, 2023, **75**, 2200191.
3 F. Khan, A. B. Siddique, M. I. Irfan, M. N. u. Hassan, M. Sher, H. A. Alhazmi, A. N. Qramish, H. M. Amin, R. Qadir and A. Abbas, *Water, Air, Soil Pollut.*, 2024, **235**, 536.
4 A. B. Siddique, M. A. Shaheen, S. Shafeeq, A. Abbas, Y. Zaman, Z. Ishaque and M. Aslam, *Mater. Adv.*, 2025, **6**(4), 1330–1344.
5 A. B. Siddique, M. A. Shaheen, A. Abbas, Y. Zaman, M. Z. Ishaque, A. Shami, M. Aslam, K. M. Alsyaad and A. Ali, *J. Mol. Struct.*, 2025, **1331**, 141566.
6 A. Rafiq, M. Ikram, S. Ali, F. Niaz, M. Khan, Q. Khan and M. Maqbool, *J. Ind. Eng. Chem.*, 2021, **97**, 111–128.
7 R. Sattara, M. Rasoola, R. Qadirb, A. Siddiqueb, M. Irfanb, I. Sabac, M. Akhtarb, M. ur Rehmana and M. Mustaqeemb, *J. Optoelectron. Biomed. Mater.*, 2023, **15**, 1–9.
8 M. I. Irfan, M. Sadiq, L. Zohra, A. B. Siddique, M. Yousaf, M. Rubab, K. Urooj, A. Aziz, H. Ali and M. Fatima, *J. Water Process Eng.*, 2024, **68**, 106337.
9 A. B. Siddique, M. A. Shaheen, A. Abbas, Y. Zaman, M. U. Rasheed, A. Karim, M. Mustaqeem, M. M. Alam and A. S. Alahmari, *Water, Air, Soil Pollut.*, 2025, **236**, 1–22.
10 G. Murugadoss, R. K. Manavalan, N. Venkatesh, G. Thiruppathi, P. Sundararaj, D. Murugan and K. Kirubaharan, *Mater. Sci. Eng., B*, 2025, **316**, 118148.
11 X. Zhang, S. Yan, R. Tyagi and R. Surampalli, *Chemosphere*, 2011, **82**, 489–494.
12 J. S. Shukla, *Environmental Applications of Nanotechnology*, Academic Guru Publishing House, 2024.
13 A. B. Siddique, M. A. Shaheen, A. Abbas, Y. Zaman, M. A. Bratty, A. Najmi, A. Hanbashi, M. Mustaqeem, H. A. Alhazmi and Z. ur Rehman, *Heliyon*, 2024, **10**, e40679.
14 P. Nayak, S. Kumar, I. Sinha and K. K. Singh, *Environ. Sci. Pollut. Res.*, 2019, **26**, 16279–16288.
15 A. A. M. Sakib, S. M. Masum, J. Hoinkis, R. Islam and M. A. I. Molla, *J. Compos. Sci.*, 2019, **3**, 91.
16 R. Saravanan, S. Karthikeyan, V. Gupta, G. Sekaran, V. Narayanan and A. Stephen, *Mater. Sci. Eng., C*, 2013, **33**, 91–98.
17 N. Abraham, C. Unni and D. Philip, *J. Mater. Sci.: Mater. Electron.*, 2018, **29**, 21002–21013.
18 M. Tariq, Y. Zaman, M. Shahzad, K. Ahmad, A. B. Siddique and H. Zaman, *Mater. Sci. Eng., B*, 2023, **294**, 116549.
19 M. Jeevarathinam and I. Asharani, *Sci. Rep.*, 2024, **14**, 9718.
20 V. U. Siddiqui, A. Ansari, M. T. Ansari, M. K. Akram, W. A. Siddiqi, A. M. Alosaimi, M. A. Hussein and M. Rafatullah, *Catalysts*, 2021, **11**, 1509.
21 A. G. Bekru, L. T. Tufa, O. A. Zelekew, M. Goddati, J. Lee and F. K. Sabir, *ACS Omega*, 2022, **7**, 30908–30919.
22 A. B. Siddique, M. A. Shaheen, A. Abbas, Y. Zaman, A. Ali, M. Naeem-ul-Hassan and J. Iqbal, *J. Environ. Chem. Eng.*, 2024, **12**, 112725.
23 K. Madeshwaran and R. Venkatachalam, *J. Ind. Eng. Chem.*, 2024, **140**, 454–467.
24 D. Thatikayala and B. Min, *J. Mater. Sci.: Mater. Electron.*, 2021, **32**, 17154–17169.
25 Y.-P. Liang, Y.-B. Chan, M. Aminuzzaman, M. Shahinuzzaman, S. Djearamane, K. Thiagarajah, S.-Y. Leong, L.-S. Wong and L.-H. Tey, *Catalysts*, 2025, **15**, 275.
26 Y. J. Wong, H. Subramaniam, L. Shing Wong, A. C. T. A. Dhanapal, Y. B. Chan, M. Aminuzzaman,

L.-H. Tey, A. K. Janakiraman, S. Kayarohanam and S. Djearamane, *Green Process. Synth.*, 2024, **13**, 20240164.
27 Y. B. Chan, M. Aminuzzaman, Y. F. Win, S. Djearamane, L. S. Wong, S. K. Guha, H. Almohammadi, M. Akhtaruzzaman and L.-H. Tey, *Catalysts*, 2024, **14**, 486.
28 Y. B. Chan, M. Aminuzzaman, L.-H. Tey, Y. F. Win, A. Watanabe, S. Djearamame and M. Akhtaruzzaman, *Materials*, 2023, **16**, 5421.
29 Y. B. Chan, M. Aminuzzaman, X.-T. Chuah, K. Li, P. Balu, L. S. Wong, S. K. Guha and L.-H. Tey, *Nanotechnol. Rev.*, 2025, **14**, 20250157.
30 J. Manoharan, N. K. Chinnakannu and B. Ranganathan, *Res. J. Pharm. Technol.*, 2023, **16**, 4831–4835.
31 N. Nadeem, A. Habib, S. Hussain, A. Sufian, I. Ahmad, F. Noreen, A. Mehmood, F. Ali, K. M. Batoo and M. F. Ijaz, *J. Inorg. Organomet. Polym.*, 2025, **35**, 1036–1051.
32 J. Dolai, K. Mandal and N. R. Jana, *ACS Appl. Nano Mater.*, 2021, **4**, 6471–6496.
33 M. T. Maru, B. A. Gonfa, O. A. Zelekew, S. P. Fakrudeen, H. Ananda Murthy, E. T. Bekele and F. K. Sabir, *Green Chem. Lett. Rev.*, 2023, **16**, 2232383.
34 S. N. H. Gardezi, M. T. Akhtar, R. Qadir, M. Mustaqeem, S. Batool, A. B. Siddique, H. Alhumade, M. H. Tahir and M. Saadia, *ACS Omega*, 2022, **7**, 47755–47763.
35 M. Z. Ishaque, Y. Zaman, Y. Yousaf, M. Shahzad, A. B. Siddique, H. Zaman, S. Ali and N. Ali, *Water, Air, Soil Pollut.*, 2024, **235**, 43.
36 A. Shah, S. Akhtar, F. Mahmood, S. Urooj, A. B. Siddique, M. I. Irfan, M. Naeem-ul-Hassan, M. Sher, A. Alhoshani and A. Rauf, *Surf. Interfaces*, 2024, **51**, 104556.
37 A. B. Siddique, M. A. Shaheen, A. Abbas, Y. Zaman, H. M. Amin, M. M. Alam, N. K. Alharbi, F. Alshehri, A. Shami and F. A. Al-Joufi, *Int. J. Environ. Anal. Chem.*, 2025, 1–23.
38 Z. Khalid, A. Ali, A. B. Siddique, Y. Zaman, M. F. Sibtain, A. Abbas, M. M. Alam and M. S. Alwethaynani, *RSC Adv.*, 2025, **15**, 16879–16893.
39 K. Mubeen, A. Irshad, A. Safeen, U. Aziz, K. Safeen, T. Ghani, K. Khan, Z. Ali, I. ul Haq and A. Shah, *J. Saudi Chem. Soc.*, 2023, **27**, 101639.
40 A. Ejaz, Z. Mamtaz, I. Yasmin, M. Shaban, A. B. Siddique, M. I. Irfan, A. Ali, S. Muhammad, M. Y. Sameeh and A. Abbas, *J. Mol. Liq.*, 2024, **393**, 123622.
41 R. Kaur, M. Suresh, J. López-Vidrier, S. Gutsch, C. Weiss, M. Prescher, L. Kirste, R. Singh, B. Pal and M. Zacharias, *New J. Chem.*, 2020, **44**, 19742–19752.
42 S. Ullah, M. Shaban, A. B. Siddique, A. Zulfiqar, N. S. Lali, M. Naeem-ul-Hassan, M. I. Irfan, M. Sher, M. F. ur Rehman and A. Hanbashi, *J. Environ. Chem. Eng.*, 2024, **12**, 113350.
43 S. Kamble, S. Agrawal, S. Cherumukkil, V. Sharma, R. V. Jasra and P. Munshi, *ChemistrySelect*, 2022, **7**, e202103084.
44 Y. Zaman, M. Z. Ishaque, K. Waris, M. Shahzad, A. B. Siddique, M. I. Arshad, H. Zaman, H. M. Ali, F. Kanwal and M. Aslam, *Arabian J. Chem.*, 2023, **16**, 105230.
45 J. O. Ighalo, P. A. Sagboye, G. Umenweke, O. J. Ajala, F. O. Omoarukhe, C. A. Adeyanju, S. Ogunniyi and A. G. Adeniyi, *Environ. Nanotechnol., Monit. Manage.*, 2021, **15**, 100443.
46 P. Jayaram, P. Pradyumnan and S. Z. Karazhanov, *Phys. B*, 2016, **501**, 140–145.